An energy-dependent earthquake moment-frequency distribution

Spassiani Ilaria[†,⋆] and Marzocchi Warner[‡]

[†]Corresponding author. *Email address*: ilaria.spassiani@ingv.it

[⋆]Istituto Nazionale di Geofisica e Vulcanologia (INGV), Roma, Italy

[‡]The University of Naples Federico II, Naples, Italy

Submitted to BSSA

Abstract

The magnitude-frequency distribution (MFD) of many earthquake catalogs is well described by the Gutenberg-Richter (GR) law, or its tapered version (TGR). This distribution is usually extrapolated to any subsets of the space-time window covered by the catalog. However, some empirical observations and logical thoughts may raise doubts about the validity of this extrapolation. For example, according to the elastic rebound theory, we may assert that the probability of a strong shock to nucleate within a short time-interval in a small area $\mathcal{A}$ just ruptured by another strong event, should be lower than that expected by GR (or TGR): a lot of energy has already been released, and it takes time to recover to the previous state. Here we put forward a space-time modification of the TGR, named TGRE (energy-dependent TGR), where the corner seismic moment becomes a time-varying energy function depending on: i) the conceivable strongest shock that may nucleate in $\mathcal{A}$; ii) the time elapsed since the last strong earthquake resetting the elastic energy in $\mathcal{A}$ to a residual value; iii) the rate of the energy recovering, linked to the recurrence time of the fault(s) involved. The model also verifies an invariance condition: for large space-time windows the occurrence of a strong shock doesn't affect significantly the whole elastic energy available, i.e., the TGRE becomes the TGR. The model is simple and rooted in clearly stated assumptions. To evaluate its reliability and applicability, we apply it to the Landers sequence in 1992. As expected by TGRE, we find that the MFD close to the fault system interested by the mainshock (Mw7.3) differs from that of earthquakes off-fault, showing a lower corner magnitude. We speculate that TGRE may be profitably used in operational earthquake forecasting, and explains the empirical observation that strongest aftershocks nucleate always outside the

mainshock fault.

Introduction

The Gutenberg-Richter (GR) law (Gutenberg and Richter (1944)) and its tapered version (TGR) (Kagan (2002a,b)) are the most used magnitude-frequency distributions (MFD) at quite different space-time windows, such as, for example, in operational earthquake forecasting models (Jordan et al. (2011); Marzocchi et al. (2017); Omi et al. (2018); Michael et al. (2019)). The validity of the (T)GR rests on the assumption that the magnitude of an earthquake is independent from the past seismicity for any dimension of the space-time window. Although this assumption seems appropriate when looking at large spatiotemporal domains, its validity at small space-time scales conflicts with some empirical findings, for which the largest triggered events occur outside the fault of the strong triggering earthquake (van der Elst and Shaw (2015); Stallone and Marzocchi (2019)).

Conceptually, this empirical observation could be explained in the framework of the elastic rebound theory (Reid (1911)), for which one strong earthquake decreases significantly the elastic energy available in the fault that generates the shock, and it takes time to recover it. This means that the probability of a strong shock to nucleate in the same area where another strong earthquake just occurred within a short-time window, has to be lower than that predicted by the (T)GR law. Conversely, if we consider a larger spatial scale, the occurrence of a single shock does not affect significantly the elastic energy available in the area, so it is expected that the (T)GR keeps holding. Besides the empirical evidence, we notice that the existence of a possible variability of MFD stems from recent operational earthquake forecasting models (Field et al. (2017a,b)), based on faults system which can produce reliable forecasts only when the MFD is changed in space.

In this paper we put forward a space-time dependent model, which describes the MFD of earthquakes that nucleate in small space-time areas, taking into consideration the elastic energy released by the past seismicity in that area. The use of a small space-time dimension marks the difference with very recent studies on a similar argument (Marsan and Tan (2020)), and with past analyses on the definition of the maximum magnitude expected in fixed (long) time windows (Zöller et al. (2013)). The model introduces a time-varying corner seismic moment in the TGR law, which results from the level of elastic energy that is currently available to be released in the space-time area of interest. We name the model TGRE to explicitly reflect the dependence of the MFD on the elastic energy available. In a nutshell, TGRE inhibits the nucleation of large earthquakes in the area that just experienced a significant release of elastic energy.

An alternative apporach to model the space-time variability of the elastic energy available is based on quantifying space-time variations of the b-value parameter in the GR law (Gulia and Wiemer (2019)). For instance, a larger b-value diminishes the probability of large earthquakes, but they still remain possible (e.g., if we keep fixed the rate of M4+ earthquakes, increasing the b-value from 1.0 to 1.2 diminishes the M7+ rate of a factor of about 4). Empirical evidence seems to show that this chance is maybe lower, because large aftershocks nucleate almost exclusively in the outer regions of the mainshock zone (van der Elst and Shaw (2015)). The model that we put forward in this study is likely more suitable to explain such empirical evidence.

In the first part of this paper we describe the theoretical aspects of the model: we explicitly derive its formulation and that of the time-varying corner seismic moment with respect to which it is conditioned; we also discuss the stability conditions in comparison with that of the classical GR model. In the second part we analyze the Landers earthquake sequence, started on June 28, 1992, with a Mw7.3 event, with a dual purpose: i) to find empirical evidence corroborating the existence of space-time variability of the MFD; ii) to test if the proposed TGRE model better describes the data than the space-time independent TGR model.

The energy-dependent MFD model (TGRE)

For the sake of mathematical simplicity, the TGRE is built in terms of seismic moment instead of magnitude; the transition from one to the other can be easily made by applying Kanamori (1977)'s relationship $m = \frac{2}{3}\log M - 10.73$, where M stays for seismic moment (in dyne $\times$ cm) and m for the corresponding moment magnitude. Such a notation will be adopted in this paper hereafter; furthermore, owing to the unambiguous relationship above, we will use the acronym MFD also for the seismic moment-frequency distribution. The MFD Tapered Pareto GR (TGR) law introduced by Kagan (2002a,b) reads:

$$\Phi_{TGR}(M) = \Phi_{GR}(M) \cdot \exp\left\{\frac{M_{min} - M}{M_c}\right\}, \tag{1}$$

where $\Phi_{GR}(M) = \left(\frac{M}{M_{min}}\right)^{-\beta_k}$ is the GR-distribution, $\beta_k = \frac{2}{3}b$-value, M_{min} is the completeness threshold and M_c is the corner seismic moment, which is the value such that events with a higher seismic moment are less likely than what expected by the decreasing exponential distribution. The tail of the GR law is therefore forced to decay stronger in the TGR model, the decay itself being controlled by the M_c value which is assumed as a fixed parameter, typically estimated through the maximum likelihood technique (Kagan and Schoenberg (2001)).

In this paper we introduce the TGRE model for earthquakes which nucleate inside an arbitray portion $\mathcal{A}$ of the fault (the generalization to a volume is straightforward). The TGRE model relaxes the hypothesis that M_c is a fixed parameter, and it allows it to vary as a function of the amount of energy E currently available in $\mathcal{A}$, i.e., $M_c \equiv M_c(E, t)$, where t is the time since the last earthquake which resets the energy in $\mathcal{A}$ to a minimum value. This function $M_c(E, t)$ has to consider the past earthquakes that nucleated in $\mathcal{A}$, as well as the earthquakes that involved $\mathcal{A}$ in their rupture nucleated somewehere else (we use the term "participation" hereafter as in Parsons et al. (2018)). In this way, the TGRE model inhibits a second strong shock to nucleate in a small area that has been involved in a strong earthquake recently, but it does not prevent this area to participate to the rupture of another big event which may nucleate nearby, along the same fault(s) involved. It follows that the nucleation MFDs in two nearby small areas may be different, but still influenced by the reciprocal seismicity. For the sake of simplicity, hereafter we will omit to specify the dependence on t in the notation of $M_c(E)$.

We also constrain the model to respect a sort of "invariance condition", i.e., the

TGRE turns back to the classical TGR at large spatiotemporal scales. Of course, the specific choice of considering a time-varying corner seismic moment is not the only one possible to introduce an energy-dependece in the MFD, but it is justified in terms of easily practical use and testing; any other way of including a direct dependence on the energy can be proposed, provided that a higher complexity must be worth for a better reliability of the model, and coherence with previous pieces of evidence is needed. In the following subsections we define both the time-varying corner seismic moment $M_c(E)$, and the explicit distribution of the TGRE model.

Time-varying corner seismic moment $M_c(E)$

Here we propose a formulation of $M_c(E)$ based on two main concepts. First, the relevant quantities controlling the earthquake nucleation in $\mathcal{A}$ are: the strongest earthquake that can eventually nucleate in $\mathcal{A}$, and the most recent past earthquake which resets the available energy to the residual minimum value. Specifically, the elastic energy in $\mathcal{A}$ is reset when this area participates to an earthquake which nucleates outside, or when an earthquake nucleates inside and generates a fractured area larger than $\mathcal{A}$. In other words, the resetting event must have a seismic moment $M \geq M_A$, where M_A is the seismic moment of an earthquake with area equal to $\mathcal{A}$. To determine if an event has involved this area, we check if at least part of $\mathcal{A}$ falls in the CircleArea with the earthquake epicenter. The relative diameter (as well as M_A) may be computed through any proper RuptureLength-MomentMagnitude relationship such as in Wells and Coppersmith (1994), Papazachos et al. (2004), or Allen and Hayes (2017).

Second, the elastic energy available in $\mathcal{A}$ scales with times and it is related to M_c. In elasticity theory, $E \propto \sigma^2$, where E is the elastic energy accumulated as a consequence of the applied stress σ; since the stress rate due to plate tectonics can be considered a constant value (that is, $\sigma \propto t$), it follows that $E \propto t^2$. The link between elastic energy available and seismic moment is instead more controversial. In a general way, $E \propto M_c$ holds only if the static stress drop of earthquakes is independent from the magnitude. This hypothesis is still matter of intense debate (Ide and Beroza (2001); Kanamori and Brodsky (2004); Oth et al. (2010)). In this paper we assume that elastic energy available and seismic moment are proportional. At the same time we stress that a similar TGRE may be built adopting a different form of $M_c(E)$, which takes into account a different hypothesis.

Going into the detail, we define the following parameters.

a) M_c^* is the maximum corner seismic moment, i.e., the seismic moment of the conceivable strongest shock that may nucleate in $\mathcal{A}$. It is actually the corner seismic moment M_c adopted in the classical TGR distribution (1). We propose that M_c^* could be related, even though not necessarily, to the length of the longest fault included in the area: for instance, it can be obtained from any proper RuptureLength-MomentMagnitude relationship, such as those proposed in Wells and Coppersmith (1994), Papazachos et al. (2004), or Allen and Hayes (2017).

b) t_0 is the occurrence time of the earthquake which has reset the elastic energy in $\mathcal{A}$, i.e., the past earthquake at which $\mathcal{A}$ participated.

c) $M_{c,0}^*$ sets the minimum value for the corner seismic moment which is achieved after the occurrence of a resetting earthquake in $\mathcal{A}$. In general, $M_{c,0}^* = \rho \cdot M_c^*$, where $\rho < 1$ indicates the fraction of elastic energy that is available after the resetting event. The value of ρ, or equivalently of $M^*_{c,0}$, may be either set theoretically, for instance by analyzing the stress rotation (Hardebeck and Okada (2018)), or empirically, by analyzing one or more stacked similar earthquake sequences.

d) ν is a parameter connected to the recurrence time of the longest fault involved in $\mathcal{A}$, and it controls the velocity of convergence to the maximum value M^*_c after a resetting event.

In "Application to real earthquakes: the Landers sequence", subsection "Setting parameters and assumptions", we describe some practical choices of these parameters. Still, we stress again that the choices are not prescriptive for the TGRE's application; different $M_c(E)$ parameterizations, assumptions and parameters can be used.

According to the above concepts and definitions, we define the time-varying energy function as

$$M_c(E) \;=\; M^*_{c,0} + (M^*_c - M^*_{c,0})\,[\nu(t - t_0)]^\alpha \tag{2}$$

bounded to the values $(t-t_0) \leq \frac{1}{\nu}$, which translates in $(t-t_0) \leq \tau$ when the coefficient of variation of the interevent times between consecutive earthquakes (CoV) is zero, i.e., τ is the recurrence time between earthquakes. This restriction guarantees indeed that $M_c(E) \in [M^*_{c,0}, M^*_c)$ when $(t - t_0) \in [0, \tau]$, a requirement that is deducible from the argument above. The dependence on time of the corner seismic moment is therefore expressed with respect to the time elapsed since the resetting event, and the seismic moments multiplication term allows us to account for the energy reloading process; while, $M^*_{c,0}$ is added to ensure that the available energy will not fall below its minimum value, even immediatly after the resetting event, that is, when $t-t_0 \sim 0$. In this paper, according to the proportionality between elastic energy and seismic moment, we set $\alpha = 2$ ($\alpha = 1$ if the seismic moment is assumed to increase linearly with time).

The temporal trend of $M_c(E)$, as well as its sensitivity to the parameters, can be observed in Fig. 1, whose plots are obtained by considering two parameters among $(M_c^*, M_{c,0}^*, \nu)$ fixed, the third varying; for an easier interpretation, we also display magnitude values instead of seismic moments. An overall increasing trend is shown in all the plots. As the intuition suggests, the time-varying corner seismic moment approaches more rapidly its maximum when ν becomes larger: the lower the recurrence time of the fault, the faster M_c^* can be reached. The increasing velocity of $M_c(E)$ is also faster as M_c^* is higher, whereas it does not change with $M_{c,0}^*$. This is because the influence of the latter on the taper's trend can be appreciated only within a short-time interval since the resetting event (less than 1 year in our example), being $M_c(E)$ controlled mainly by M_c^* and ν at just larger scales: that's why the x-axes in plot c) are cut at 1 year after the reset, otherwise the difference would not have been visible. When focusing on the entire time window, we observe instead that the influence of ν and M_c^* on $M_c(E)$ is a bit stronger. However, Fig. 2 highlights that in the short-term, the time-varying corner seismic moment does not substantially depend on these two values.

To be thorough, we add that $M_c(E)$ could be also interpreted as a random variable whose distribution takes the cue from the stress level adopted in the stress release model (Vere-Jones (1978, 1988); Wang et al. (1991); Zheng and Vere-Jones (1991); Xiaogu and Vere-Jones (1994)). In fact, $M_c(E)$ could consist in a deterministic term of accumulated energy, linked to the elapsed time since the resetting event, and a stochastic term of energy released by each single past earthquake, which is distributed according to TGR. Nevertheless, so as to gain in easily applicability and reliability testing, we assume here that $M_c(E)$ is a deterministic function of time, as defined in (2).

The mathematical description of the TGRE model

The TGRE model we propose for earthquake seismic moments is simply obtained by including the time-varying corner seismic moment $M_c(E)$ previously derived, into the TGR cumulative distribution (1), i.e.,

$$\Phi_{TGRE}(M) = \left(\frac{M}{M_{min}}\right)^{-\beta_k} \exp\left\{\frac{M_{min} - M}{M_c(E)}\right\}, \tag{3}$$

where $M_c(E) \in [M^*_{c,0}, M^*_c]$ is defined in (2) with $\alpha = 2$. Fig. 3 shows $\Phi_{TGRE}(M)$ as a function of $M_c(E)$.

If we consider a large spatial domain composed by many faults, and many cells $\mathcal{A}$, the occurrence of one or a few large earthquakes may reset only a limited number of cells $\mathcal{A}$. This means that for the whole large spatial domain, $M_c(E) \equiv M^*_c$, acknowledging the spatial invariance condition. The temporal invariance condition is instead satisfied by construction in fact, equation (2) gives M^*_c for $t - t_0 \to \tau$.

One obvious application of the TGRE model is in operational earthquake forecasting (OEF; Jordan et al. (2011)). It is expected to solve the main conundrum of existing OEF models (Marzocchi et al. (2017); Omi et al. (2018); Michael et al. (2019)), for which the probability of a large aftershock is exactly where the mainshock occurred.

For example, the ETAS-TGRE (i.e., ETAS with TGRE) rate would be

$$\lambda(t,x,y,M|\mathcal{H}_t) = \left[\lambda_0(x,y) + \sum_{\{i|t_i<t\}} \lambda_{tr}(t-t_i, x-x_i, y-y_i; M_i)\right] p_{TGRE}(M|M_c(E)), \tag{4}$$

where $\mathcal{H}_t$ is the past history up to time t, i.e., the past earthquakes $\{(t_i, x_i, y_i, M_i); t_i < t\}$; $\lambda_0(x,y)$ is the rate of the background events; $\lambda_{tr}(t-t_i, x-x_i, y-y_i; M_i)$ is the rate of the triggered events; $p_{TGRE}(M|M_c(E))$ is the TGRE probability density function for the seismic moment that is calculated in x, y at the time t; finally, $M_c(E) \equiv M_c(E, x, y, s)$ is linked to the elastic energy available in x, y after a time s since the last resetting earthquake. In this framework, the TGRE may be applied to both the background and triggered earthquakes as in the classical ETAS model.

In the ETAS-TGRE setting, it is also interesting to investigate how the shift of the TGRE taper influences the computation of the branching ratio, which we recall being the average number of aftershocks triggered by an arbitrary event (Zhuang et al. (2012)). As for the TGR law, the branching ratio of the TGRE model can be derived as

$$\eta_{TGRE} = \kappa + \kappa \alpha_k e^{\frac{M_{min}}{M_c(E)}} \left(\frac{M_{min}}{M_c(E)}\right)^{\beta_k - \alpha_k} \Gamma\left(-\beta_k + \alpha_k, \frac{M_{min}}{M_c(E)}\right), \tag{5}$$

where $\Gamma(s,t) = \int_t^\infty x^{s-1} e^{-x} dx$ is the upper incomplete Gamma function (Bateman (1953); Temme (1996); Spassiani (2020)), and κ, α_k are the parameters of the productivity law $\varrho(\cdot)$ expressed in terms of the seismic moment through Kanamori (1977)'s relationship, i.e., $\varrho(M) = \kappa \left(\frac{M}{M_{min}}\right)^{\alpha_k}$. In Fig. 4 we show that η_{TGRE} increases with the time-varying corner seismic moment $M_c(E)$, indicating that if the taper moves to the left as a consequence of a great amount of energy just released, the average number of aftershocks triggered by a generic event is reduced: in fact, an event with a lower seismic moment will generate a lower number of aftershocks. The plot shows that the increasing behavior is faster as the difference $\beta_k - \alpha_k$ is lower: in the case of the classical ETAS-GR it has to be $\beta_k > \alpha_k$ for the process not to explode, but this condition becomes unnecessary for the ETAS-TGRE model, so as for ETAS-TGR (Spassiani (2020)). As usual, the stability of the ETAS-TGRE process is guaranteed by imposing $\eta_{TGRE} < 1$; finally, when $\beta_k > \alpha_k$ it holds $\eta_{TGRE} < \eta_{GR}$, therefore in this case our model's stability conditions are even less restrictive than those of ETAS-GR.

Application to real earthquakes: the Landers sequence

In this section we test the hypothesis of the space and time independence of MFD, and then we show how the TGRE model works in practice. To do that, we consider the Landers earthquake sequence, which started with a magnitude Mw7.3 event occurred on June 28, 1992, in Southern California. The seismic catalog for such a sequence is rich enough to allow a statistically significant data-model comparison. Furthermore, the fault segment that generates the initial earthquake is well-defined in this case, as a detailed mapping of the slip distribution is available: in our analysis we focus on the fault segments that certainly slipped during the Mw7.3 event, as shown in Madden and Pollard (2012) and hereafter called "Landers fault".

Seismic data for the analysis have been taken from the online available Uniform California Earthquake Rupture Forecast, version 3 (UCERF3) earthquake catalog, which covers the entire California Region from July 1769 to April 2010 and includes events with mag ≥ 4 before 1894 and mag ≥ 2.5 after this year (Field et al. (2013)). The data relative to the Landers fault have instead been taken from the California Reference Fault Parameter Database (CRFPD)-UCERF2 system, that is easily accessible online (Field et al. (2009)) and does not present substantial differences with respect to the UCERF3 regarding the faults involved by the Landers rupture. For the websites, see "Data and Resources".

In particular, in this application we test whether the MFDs inside and outside the rupture that generates the Landers earthquake come from the same distribution, as it would be expected in the case of space-time independence. Then, we apply the TGRE model to the on-rupture earthquakes, and we quantify the difference of the reliability of the TGR and TGRE models through the log-likelihood ratio test. The red stripe in panels a) of figures from 5 to 8 shows the rupture on the Landers fault. The stripe has a thickness of about 10 km (considering ± 5 km around the latitude of each segment fault point). The analysis is conducted in the following four time intervals: 29 June - 6 July 1992, 29 June - 29 July 1992, 29 June - 29 September 1992, 29 June 1992 - 29 June 1993, that is, respectively 1 week, 1 month, 3 months and 1 year since the day after the Mw7.3 resetting event.

Setting parameters and assumptions

The first step is to define $\mathcal{A}$, which sets the spatial resolution of the analysis. We consider the case in which $\mathcal{A}$ covers the whole fault rupture of the Mw7.3 earthquake (red stripes in panels a) of figures from 5 to 8). For this tutorial application we set the parameters of the TGRE model as follows.

i) M_c^* corresponds to $m_c^* = 7.59$, as proposed in Kagan et al. (2010) for active continents.

ii) After the resetting Landers earthquake, no other resetting earthquake occurred in $\mathcal{A}$ in the time interval considered, therefore t_0 corresponds to June 28, 1992.

iii) $M_{c,0}^*$ is estimated through a grid search; specifically, we search the $m_{c,0}^*$ in the set $[4, 4.1, \ldots, 6]$ which maximizes the likelihood ratio in favour of TGRE in the first week of data. As shown in Fig. 9, we find $m_{c,0}^* = 4.3$. Of course, more sophisticated procedures to estimate $M_{c,0}^*$ are possible, but we argue that the results are stable for reasonable variations of this parameter. In particular, the log-likelihood ratio remains well above zero (TGRE explains the data better than TGR) for $4.1 \leq m_{c,0}^* = 4.3 \leq 4.8$. Then, in Table 1 we show also that the $M_{c,0}^*$ estimated in the first week of data brings to a superiority of TGRE with respect to TGR also for other time windows (1 month, 3 months, and 1 year) (see section "Results" for more details).

iv) $\nu = \frac{1}{\tau(1-2cov)}$, where the recurrence time $\tau = 250$ years is rescaled accounting for the covariance coefficient CoV= 0.3.

The results are illustrated in the next section. To check their stability and the sensitiveness of the model, besides using different $M_{c,0}^*$, we perform the analysis also for other possible values of the parameters M_c^* and τ. The details are reported in the caption of Table 1. We anticipate that the results are not significantly modified, in agreement with what shown in Fig. 2 previously discussed.

Results

Results are illustrated in figures from 5 to 8, respectively for 1 week, 1 month, 3 months and 1 year since the day after the resetting Landers event. The space-time windows in which the analysis is performed are shown in the map of panels *a*), where the on-rupture seismicity of $\mathcal{A}$ (red dots) is reported inside the red stripe.

In panels *b*) of figures from 5 to 8, we show the results of the null hypothesis of having the same MFD inside and outside the ruptured area. In particular, we plot the earthquake cumulative numbers of events inside (in red) and outside (in dark blue) $\mathcal{A}$ in different time windows. In each of the four temporal intervals, red and dark blue step functions are clearly different, and the two-samples Kolmogorov-Smirnov test (Massey (1951)) confirms the rejection of the null hypothesis that the data are drawn from the same continuous distribution, with a $p-value$ much smaller than the 1% significance level chosen before carrying out the analysis. We stress that these results are completely independent of the modeling, as they are obtained by considering only earthquake data. At the same time, these results support the main motivation of this work, i.e., empirical data support the hypothesis of different MFDs on- and off-rupture just after a large shock.

Panels *c*) in all the figures from 5 to 8 show the goodness-of-fit of the TGRE and TGR models with respect to the earthquake data inside $\mathcal{A}$. Specifically, we plot the TGR model in black versus the TGRE one in yellow, orange, green and blue respectively for 1 week (Fig. 5), 1 month (Fig. 6), 3 months (Fig. 7) and 1 year (Fig. 8) since the reset. We also show 1000 simulations of 1000 magnitudes each, obtained both with $m_c^* = 7.59$, that is drawn from a TGR (light gray cones), and with the new corner magnitudes $m_c(E)$ obtained for the TGRE model (light yellow, orange, green and blue cones for the four temporal intervals considered). Results show that within one week since the Landers earthquake, the TGRE corner seismic moment is reduced to a value $\sim M_{c,0}^*$ corresponding to the minimum energy, and after that it increases with the energy reloading process.

In all the four cases, the TGRE model gives visually a better fit to earthquake data than the TGR model: the red step functions representing the recorded magnitudes are almost completely contained in the non-gray cones, indicating our model's capability to better reproduce the time evolution of the real seismicity occurred in $\mathcal{A}$ that just experienced the strong resetting Landers event. We argue that this general observation is independent from the choice on $M_{c,0}^*$, because of the clear bending in the MFD of the earthquakes inside $\mathcal{A}$.

We explore further the suitability of TGRE calculating the likelihood ratio for the nested TGR and TGRE models (King (1998)). The likelihood ratio is a measure of how much the TGRE is supported by the data with respect to TGR. In particular, the log-likelihood function

$$log\, L(\theta) = N\beta_k \log M_{min} + \frac{NM_{min} - \sum_{i=1}^{N} M_i}{\theta} + \sum_{i=1}^{N} \log\left(\frac{\beta_k}{M_i} + \frac{1}{\theta}\right) - \beta_k \sum_{i=1}^{N} \log M_{min} \tag{6}$$

is the same for both the models, and it represents the TGRE when $\theta = M_c(E)$, and the TGR when $\theta = M_c^*$. In Table 1 we show the difference $log\, L(M_c(E)) - log\, L(M_c^*)$ between the two log-likelihoods, computed for the four space-time windows considered above. The results in the first row of Table 1 are relative to the earthquake data used in figures from 5 to 8, panels c), i.e., with $m_c^* = 7.59$, $m_{c,0}^* = 4.3$ and $\tau = 250$ years. As anticipated in the previous section, to verify the stability of the results as a function of these parameters, we calculate the likelihood ratio also for different m_c^* and τ (see the first three columns in Table 1); for all these cases, we found that $m_{c,0}^* = 4.3$ maximizes the likelihood ratio in favour of TGRE in the first week of data. The results of this stability test are shown in the rows from the second on. Borrowing the terminology adopted by Kass and Raftery (1995) for the Bayes factor, we may say that the evidence in favour of TGRE with respect to TGR is, most of the times, "substantial" and "strong". As expected, this evidence lowers only in some cases for a long temporal window considered, but it still remains always > 0, showing a superiority of TGRE with respect to TGR independently from the parameters. In general, the overall first-increasing-then-decreasing trend of the log-likelihood differences when moving to longer time periods is what expected, as a trade-off between the number of events and the recharging of the elastic energy of the system.

Finally, we find that the results remain stable also when considering completeness thresholds m_{min} higher than 2.5, or when removing the first few days just after the resetting Mw7.3 event, in which m_{min} may be higher than in the following days. As a matter of fact, any problem in the completeness magnitude should have equally affected the MFD of both events inside and outside $\mathcal{A}$, leaving the difference between the two distributions unchanged.

Discussion and Conclusions

Basic physical principles and empirical evidence suggest that MFD can vary with space and time. To this purpose, in this paper we have proposed the energy-varying seismic moment-frequency model TGRE for earthquake nucleation, which depends on the elastic energy currently available in an area $\mathcal{A}$ of interest. This model acknowledges the elastic rebound theory and justifies the observation that the largest triggered earthquakes nucleate always outside the fault section which has just generated a large shock. In a different perspective, the model may also describe quantitatively an intermittent criticality state that is tuned by the available elastic energy. In other words, the state of self-organized criticality (SOC) – advocated to explain the power law distribution of the seismic moments at large spatiotemporal scales (Bak and Tang (1989); Sornette and Sornette (1989)) – changes in intermittent criticality when zooming on small space-time windows which have been recently involved by a large earthquake, indicating that a fault system approaches and retreats from a critical state by turns (Ben-Zion et al. (2003); Bowman and Sammis (2004); Bebbington et al. (2010)).

The TGRE distribution is obtained as a modification of Kagan's TGR law, in which the corner seismic moment is a time-varying energy function, i.e., it is linked to the proxy of the amount of energy available in $\mathcal{A}$. The TGRE model is conceptually simple and it depends on a few parameters: i) the corner seismic moment M_c^*, which is loosely related to the strongest event that may nucleate in $\mathcal{A}$; ii) the temporal occurrence of the last large earthquake resetting the elastic energy in $\mathcal{A}$ to a residual value; iii) the rate of the energy recovering, which depends on the recurrence time of the fault(s) involved; iv) $M_{c,0}^*$, which is the minimum value for the corner seismic moment which is achieved after the occurrence of a resetting earthquake in $\mathcal{A}$. In other words, the TGRE right tail $M_c(E)$ abruptly moves to $M^*_{c,0}$ just after the occurrence of a strong (resetting) event, and then it slowly recovers to the long-term value; in practice, the model inhibits the nucleation of a large triggered earthquake in segments that recently experienced a large shock. An interesting feature of TGRE is that it verifies an invariance condition: as the dimension of the selected space-time window becomes larger, it converges to the TGR law with a limiting corner seismic moment M^*_c.

The TGRE has been designed purposedly simple (depending on a few clear physical parameters), acknowledging that understandability (and usability) is inversely proportional to the complexity of a model. Like for any other model, it contains (more or less explicit) subjective choices, but we think that these choices are less subjective than ignoring the empirical evidence that strong triggered earthquakes do not nucleate in the vicinity of a fault just ruptured by another strong event, like assumed in the (T)GR model. Note that this empirical evidence can be hardly explained by space-time variability of the b-value of the GR law, which would lower, not inhibit, the triggering of large earthquakes on a fault that has just slipped.

Despite its simplicity, we have shown that TGRE may explain well the statistically significant difference of the MFDs relative to on- and off-rupture seismicity for the Landers sequence, and that the results are stable for possible variations of the parameters. In particular, TGRE outperforms TGR for different values of $m^*_{c,0}$, showing the strongest difference for $m^*_{c,0} = 4.3$. Further studies will be necessary to reduce uncertainties on this value. For now, we just notice that the results seem to indicate that it is more important the fact that we allow the corner seismic moment to vary in space and time, rather than the details about the model's parameters choice. That said, we underline that the TGRE reliability (like for any other model) and the comparison with alternative models (e.g., models based on space-time variations of the b-value) have to be evaluated only through prospective tests. For this model, prospective tests will be carried out in the framework of the ongoing european RISE project, which supports the Collaboratory for the Study of Earthquake Predictability (CSEP) network activities in Europe (for the websites, see "Data and Resources"; (Zechar et al., 2010; Schorlemmer et al., 2018)) .

Finally, we suggest that the implementation of the TGRE may offer some benefits for operational earthquake forecasting (OEF) models, because it overcomes one of the conundrum of the best performing current clustering models (Taroni et al. (2018)), for which the likelihood of a large earthquake is exactly where another large earthquake has just occurred. This conundrum has been also identified as one of the main reasons for the instability of the forecasts produced by the UCERF3-ETAS model, which has to impose a space-time variability of the MFD to solve the problem (Field et al. (2017b)). At the same time, TGRE may also provide a different explanation of recent empirical evidence relative to variations of the b-value before and after large earthquakes close to faults (Gulia and Wiemer (2019)). In particular, although it is worth remarking that the meaning of the b-value is questionable for a distribution that is not exponential, such as the TGR, if the corner magnitude gets closer to the completeness threshold (even though the slope remains the same), the b-value necessarily increases (Marzocchi et al. (2020)).

More in general, since the use of a proper MFD may have a large impact on the earthquake predictability, we hope that this paper will stimulate further thoughts on this issue.

Data and Resources

The data used in this study are available at `http://www.wgcep.org/ucerf3`, `https://pubs.usgs.gov/of/2013/1165/` and `https://pubs.usgs.gov/of/2007/1437/` (last access, January 2019). Finally, for the RISE and CSEP projects, see respectively `www.rise-eu.org` and `https://scec.usc.edu/scecpedia/CSEP_Working_Group` (last access, April 2020).

Acknowledgments

We thank the reviewers for their useful comments and suggestions.

References

Allen, T. I., and G. P. Hayes (2017). Alternative Rupture-Scaling Relationships for Subduction Interface and Other Offshore Environments. *Bull. Seismol. Soc. Am.*, 107(3):1240–1253, March. doi: 10.1785/0120160255. URL `https://doi.org/10.1785/0120160255`.

Bak, P., and C. Tang (1989). Earthquakes as a self-organized critical phenomenon. *J. Geophys. Res. Solid Earth*, 94(B11):15635–15637. doi: 10.1029/JB094iB11p15635. URL `https://agupubs.onlinelibrary.wiley.com/doi/abs/10.1029/JB094iB11p15635`.

Bateman, H. (1953). *Higher transcendental functions.* Mc Graw-Hill Book Company, Inc.

Bebbington, M. S., D. S. Harte, and S. C. Jaumé (2010). Repeated Intermittent Earthquake Cycles in the San Francisco Bay Region. *Pure Appl. Geophys.*, 167:801–818, June. doi: 10.1007/s00024-010-0064-6.

Ben-Zion, Y., M. Eneva, and Y. Liu (2003). Large earthquake cycles and intermittent criticality on heterogeneous faults due to evolving stress and seismicity. *J. Geophys. Res. Solid Earth*, 108(B6). doi: 10.1029/2002JB002121. URL `https://agupubs.onlinelibrary.wiley.com/doi/abs/10.1029/2002JB002121`.

Bowman, D. D., and C. G. Sammis (2004). Intermittent criticality and the Gutenberg-Richter distribution. *Pure Appl. Geophys.*, 161(9):1945–1956, August. ISSN 1420-9136. doi: 10.1007/s00024-004-2541-z. URL `https://doi.org/10.1007/s00024-004-2541-z`.

Field, E. H., T. E. Dawson, K. R. Felzer, A. D. Frankel, V. Gupta, T. H. Jordan, T. Parsons, M. D. Petersen, R. S. Stein, R. J. Weldon, II, and C. J. Wills (2009). Uniform California Earthquake Rupture Forecast, Version 2 (UCERF2). *Bull. Seismol. Soc. Am.*, 99(4):2053. doi: 10.1785/0120080049. URL `http://dx.doi.org/10.1785/0120080049`.

Field, E. H., R. Arrowsmith, G. P. Biasi, P. Bird, T. E. Dawson, K. R. Felzer, D. D. Jackson, K. M. Johnson, T. H. Jordan, C. M. Madugo, A. J. Michael, K. R. Milner, M. T. Page, T. Parsons, P. Powers, B. E. Shaw, W. R. Thatcher, R. J. Weldon, and Y. Zeng (2013). Overview of the Uniform California Earthquake Rupture Forecast Version 3 (UCERF3) Time-Independent Model. *AGU Fall Meeting Abstracts*, art. S51F-04, December.

Field, E. H., T. H. Jordan, M. T. Page, K. R. Milner, B. E. Shaw, T. E. Dawson, G. P. Biasi, T. Parsons, J. L. Hardebeck, A. J. Michael, R. J. Weldon, II, P. M. Powers, K. M. Johnson, Y. Zeng, K. R. Felzer, N. van der Elst, C. Madden, R. Arrowsmith, M. J. Werner, and W. R. Thatcher (2017a). A synoptic view of the Third Uniform California Earthquake Rupture Forecast (UCERF3). *Seismol. Res. Lett.*, 88(5): 1259, October. doi: 10.1785/0220170045. URL `+http://dx.doi.org/10.1785/0220170045`.

Field, E. H., K. R. Milner, J. L. Hardebeck, M. T. Page, N. van der Elst, T. H. Jordan, A. J. Michael, B. E. Shaw, and M. J. Werner (2017b). A spatiotemporal clustering model of the Third Uniform California Earthquake Rupture Forecast (UCERF3-ETAS): Toward an operational earthquake forecast. *Bull. Seismol. Soc.*

Am., 107(3):1049, June. doi: 10.1785/0120160173. URL `http://dx.doi.org/10.1785/0120160173`.

Gulia, L., and S. Wiemer (2019). Real-time discrimination of earthquake foreshocks and aftershocks. *Nature*, 574:193–199. doi: 10.1038/s41586-019-1606-4. URL `https://doi.org/10.1038/s41586-019-1606-4`.

Gutenberg, B., and C. F. Richter (1944). Frequency of earthquakes in California. *Bull. Seismol. Soc. Am.*, 34(8):185–188, October.

Hardebeck, J. L., and T. Okada (2018). Temporal stress changes caused by earthquakes: A review. *J. Geophys. Res. Solid Earth*, 123(2):1350–1365. doi: 10.1002/2017JB014617. URL `https://agupubs.onlinelibrary.wiley.com/doi/abs/10.1002/2017JB014617`.

Ide, S. and G. C. Beroza (2001). Does apparent stress vary with earthquake size? *Geophys. Res. Lett.*, 28(17):3349–3352. doi: 10.1029/2001GL013106. URL `https://agupubs.onlinelibrary.wiley.com/doi/abs/10.1029/2001GL013106`.

Jordan, T., Y. Chen, P. Gasparini, R. Madariaga, I. Main, W. Marzocchi, G. Papadopoulos, G. Sobolev, K. Yamaoka, and J. Zschau (2011). Operational earthquake forecasting: State of knowledge and guidelines for utilization. *Ann. Geophys.*, 54, 08. doi: 10.4401/ag-5350.

Kagan, Y. Y. (2002a). Seismic moment distribution revisited: I. Statistical results. *Geophys. J. Int.*, 148(3):520–541. ISSN 1365-246X. doi: 10.1046/j.1365-246x.2002.01594.x. URL `http://dx.doi.org/10.1046/j.1365-246x.2002.01594.x`.

Kagan, Y. Y. (2002b). Seismic moment distribution revisited: II. Moment conservation principle. *Geophys. J. Int.*, 149(3):731–754. ISSN 1365-246X. doi: 10.1046/j.1365-246X.2002.01671.x. URL http://dx.doi.org/10.1046/j.1365-246X.2002.01671.x.

Kagan, Y. Y., and F. Schoenberg (2001). Estimation of the upper cutoff parameter for the Tapered Pareto Distribution. *J. Appl. Probab.*, 38, 01. doi: 10.1239/jap/1085496599.

Kagan, Y. Y., P. Bird, and D. D. Jackson (2010). Earthquake Patterns in Diverse Tectonic Zones of the Globe. *Pure Appl. Geophys.*, 167:721–741, Jun. doi: 10.1007/s00024-010-0075-3. URL https://doi.org/10.1007/s00024-010-0075-3.

Kanamori, H. (1977). The energy release in great earthquakes. *J. Geophys. Res.*, 82(20):2981–2987. doi: 10.1029/JB082i020p02981. URL https://agupubs.onlinelibrary.wiley.com/doi/abs/10.1029/JB082i020p02981.

Kanamori, H., and E. E. Brodksy (2004). The physics of earthquakes. *Rep. Prog. Phys.*, 67(8):1429. doi: 10.1088/0034-4885/67/8/r03. URL https://iopscience.iop.org/article/10.1088/0034-4885/67/8/R03.

Kass, R. E., and A. E. Raftery (1995). Bayes Factors. *J. Am. Stat. Assoc.*, 90(430):773–795. ISSN 01621459. URL http://www.jstor.org/stable/2291091.

King, G. (1998). *Unifying Political Methodology: The Likelihood Theory of Statistical Inference*. University of Michigan Press, Ann Arbor. URL http://www.press.umich.edu/titleDetailDesc.do?id=23784.

Madden, E., and D. Pollard (2012). Integration of surface slip and aftershocks to constrain the 3d structure of faults involved in the M 7.3 Landers earthquake, Southern California. *Bull. Seismol. Soc. Am.*, 102:321–342, 02. doi: 10.1785/0120110073.

Marsan, D., and Y. J. Tan (2020). Maximum Earthquake Size and Seismicity Rate from an ETAS Model with Slip Budget. *Bull. Seismol. Soc. Am.*, 0037–1106. doi: 10.1785/0120190196. URL +https://doi.org/10.1785/0120190196.

Marzocchi, W., M. Taroni, and G. Falcone (2017). Earthquake forecasting during the complex Amatrice-Norcia seismic sequence. *Sci. Adv.*, 3(9). doi: 10.1126/sciadv.1701239. URL http://advances.sciencemag.org/content/3/9/e1701239.

Marzocchi, W., I. Spassiani, A. Stallone, and M. Taroni (2020). Erratum to: How to be fooled searching for significant variations of the b-value. *Geophys. J. Int.*, 221(1): 351–351. doi: 10.1093/gji/ggaa061. URL https://doi.org/10.1093/gji/ggaa061.

Massey, F. J. Jr. (1951). The Kolmogorov-Smirnov test for goodness of fit. *J. Am. Stat. Assoc.*, 46(253):68–78. doi: 10.1080/01621459.1951.10500769. URL https://www.tandfonline.com/doi/abs/10.1080/01621459.1951.10500769.

Michael, A. J., S. K. McBride, J. L. Hardebeck, M. Barall, E. Martinez, M. T. Page, N. van der Elst, E. H. Field, K. R. Milner, and A. M. Wein (2019). Statistical Seismology and Communication of the USGS Operational Aftershock Forecasts for the 30 November 2018 Mw 7.1 Anchorage, Alaska, Earthquake. *Seismol. Res. Lett.*, 91(1): 153–173. doi: 10.1785/0220190196. URL https://doi.org/10.1785/0220190196.

Omi, T., Y. Ogata, K. Shiomi, B. Enescu, K. Sawazaki, and K. Aihara (2018). Implementation of a real-time system for automatic aftershock forecasting in Japan. *Seismol. Res. Lett.*, 90(1):242–250.

Oth, A., D. Bindi, S. Parolai, and D. Di Giacomo (2010). Earthquake scaling characteristics and the scale-(in)dependence of seismic energy-to-moment ratio: Insights from KiK-net data in Japan. *Geophys. Res. Lett.*, 37(19):L19304 doi: {10.1029/2010GL044572},\newblockURL\url https://agupubs.onlinelibrary.wiley.com/doi/abs/10.1029/2010GL044572,

Papazachos, B., E. Scordilis, D. Panagiotopoulos, C. Papazachos, and G. Karakaisis (2004). Global relations between seismic fault parameters and moment magnitude of earthquakes. *Bull. Geol. Soc. Greece*, 36(3):1482–1489, 10. doi: 10.12681/bgsg.16538. URL `https://ejournals.epublishing.ekt.gr/index.php/geosociety/article/view/16538`.

Parsons, T., E. L. Geist, R. Console, and R. Carluccio (2018). Characteristic earthquake magnitude frequency distributions on faults calculated from consensus data in California. *J. Geophys. Res. Solid Earth*, 123(12):10,761–10,784. doi: 10.1029/2018JB016539. URL `https://agupubs.onlinelibrary.wiley.com/doi/abs/10.1029/2018JB016539`.

Reid, H. F. (1911). The elastic-rebound theory of earthquakes. *Univ. Calif. Publ.. Bull. Dept. Geol.*, 6(19):413–444. URL `https://ci.nii.ac.jp/naid/10006706254/en/`.

Salisbury, J. B., T. K. Rockwell, T. J. Middleton, and K. W. Hudnut (2012). LiDAR and Field Observations of Slip Distribution for the Most Recent Surface Ruptures along the Central San Jacinto Fault. *Bull. Seismol. Soc. Am.*, 102(2):598–619, Apr. doi: 10.1785/0120110068. URL `https://doi.org/10.1785/0120110068`.

Schorlemmer, D., M. Werner, W. Marzocchi, T. Jordan, Y. Ogata, D. Jackson, S. Mak, D. Rhoades, M. Gerstenberger, N. Hirata, M. Liukis, P. Maechling, A. Strader, M. Taroni, S. Wiemer, J. Zechar, and J. Zhuang (2018). The Collaboratory for the Study of Earthquake Predictability: Achievements and Priorities. *Seismol. Res. Lett.*, 89(4):1305–1313. doi: 10.1785/0220180053. URL `https://doi.org/10.1785/0220180053`.

Sieh, K., L. Jones, E. Hauksson, K. Hudnut, D. Eberhart-Phillips, T. Heaton, S. Hough, K. Hutton, H. Kanamori, A. Lilje, S. Lindvall, S. F. McGill, J. Mori, C. Rubin, J. A. Spotila, J. Stock, H. K. Thio, J. Treiman, B. Wernicke, and J. Zachariasen (1993). Near-Field Investigations of the Landers Earthquake Sequence, April to July 1992. *Science*, 260(5105):171–176. doi: 10.1126/science.260.5105.171. URL `http://www.jstor.org/stable/2881298`.

Sornette, A., and D. Sornette (1989). Self-organized criticality and earthquakes. *EPL-Europhys. Lett.*, 9(3):197–202, jun. doi: 10.1209/0295-5075/9/3/002. URL `https://doi.org/10.1209/0295-5075/9/3/002`.

Spassiani, I. (2020). Stability of the Epidemic Type Aftershock Sequence model with Tapered Gutenberg- Richter distributed seismic moments. *submitted to Bull. Seismol. Soc. Am.*

Stallone, A., and W. Marzocchi (2019). Empirical evaluation of the magnitude-independence assumption. *Geophys. J. Int.*, 216(2):820–839. doi: 10.1093/gji/ggy459. URL `http://dx.doi.org/10.1093/gji/ggy459`.

Taroni, M., W. Marzocchi, D. Schorlemmer, M. Werner, S. Wiemer, J. Zechar, L. Heiniger, and F. Euchner (2018). Prospective CSEP Evaluation of 1-Day, 3-Month, and 5-Yr Earthquake Forecasts for Italy. *Seismol. Res. Lett.*, 89(4):1251–1261. doi: 10.1785/0220180031. URL `https://doi.org/10.1785/0220180031`.

Temme, N. M. (1996). *Special functions. An introduction to the classical functions of mathematical physics.* John Wiley and Sons Inc., New York.

van der Elst, N. J., and B. E. Shaw (2015). Larger aftershocks happen farther away: Nonseparability of magnitude and spatial distributions of aftershocks. *Geophys. Res. Lett.*, 42(14):5771–5778. doi: 10.1002/2015GL064734. URL `https://agupubs.onlinelibrary.wiley.com/doi/abs/10.1002/2015GL064734`.

Vere-Jones, D. (1978). Earthquake predicion - A statistician's view. *J. Phys. Earth*, 26(2):129–146. doi: 10.4294/jpe1952.26.129.

Vere-Jones, D. (1988) On the variance properties of the stress release models. *Aust. J. Stat.*, 30A(1):123–135. ISSN 1467-842X. doi: 10.1111/j.1467-842X.1988.tb00469.x. URL `http://dx.doi.org/10.1111/j.1467-842X.1988.tb00469.x`.

Wang, A.-L., D. Vere-Jones, and X. Zheng (1991). Simulation and estimation procedures for stress release model. In M. J. Beckmann, M. N. Gopalan, and R. Subramanian, editors, *Stochastic Processes and their Applications*, pages 11–27, Berlin, Heidelberg. Springer Berlin Heidelberg. ISBN 978-3-642-58201-1.

Wells, D. L., and K. J. Coppersmith (1994). New empirical relationships among magnitude, rupture length, rupture width, rupture area, and surface displacement. *Bull. Seismol. Soc. Am.*, 84(4):974. URL http://dx.doi.org/.

Xiaogu, Z., and D. Vere-Jones (1994). Further applications of the stochastic stress release model to historical earthquake data. *Tectonophysics*, 229(1):101 – 121. ISSN 0040-1951. doi: https://doi.org/10.1016/0040-1951(94)90007-8. URL http://www.sciencedirect.com/science/article/pii/0040195194900078.

Zechar, J. D., Schorlemmer, D., M. Liukis, J. Yu, F. Euchner, P. J. Maechling, and T. H. Jordan (2010). The Collaboratory for the Study of Earthquake Predictability perspective on computational earthquake science. *Concurr. Comp.-Pract. E.*, 22(12):1836–1847. doi: 10.1002/cpe.1519. URL https://onlinelibrary.wiley.com/doi/abs/10.1002/cpe.1519.

Zheng, X.-G., and D. Vere-Jones (1991). Application of stress release models to historical earthquakes from North China. *Pure Appl. Geophys.*, 135(4):559–576, Apr. ISSN 1420-9136. doi: 10.1007/BF01772406. URL https://doi.org/10.1007/BF01772406.

Zhuang, J., M. Werner, S. Hainzl, D. Harte, and S. Zhou (2012). Basic models of seismicity: Temporal models. *CORSSA*, 33.

Zöller, G., M. Holschneider, and S. Hainzl (2013). The Maximum Earthquake Magnitude in a Time Horizon: Theory and Case Studies. *Bull. Seismol. Soc. Am.*, 103 (2A):860–875, Apr. doi: 10.1785/0120120013 URL https://doi.org/10.1785/0120120013.

Authors' mailing address

Spassiani Ilaria (corresponding author)

ilaria.spassiani@ingv.it

Istituto Nazionale di Geofisica e Vulcanologia (INGV)

Via di Vigna Murata 605, 00143, Roma, Italy

Marzocchi Warner

warner.marzocchi@unina.it

University of Naples, Federico II

Dept. of Earth, Environmental, and Resources Sciences

Complesso di Monte Sant'Angelo, Via Cupa Nuova Cintia, 21

80126 Napoli, Italy

Tables

654

Table 1: Difference between TGRE and TGR log-likelihoods in bold, and $m_c(E)$ values in brackets.

			1 week	1 month	3 months	1 year
$m_c^* = 7.59$[a]	$\tau = 250$ y.[e]	$m_{c,0}^* = 4.3$	**3.16** (4.301)	**3.51** (4.32)	**2.76** (4.43)	**1.04** (4.96)
$m_c^* = 7.53$[b]	$\tau = 100$ y.[f]	$m_{c,0}^* = 4.3$	**3.15** (4.305)	**3.36** (4.38)	**1.85** (4.69)	**0.26** (5.4)
$m_c^* = 7.5$[c]	$\tau = 1000$ y.[g]	$m_{c,0}^* = 4.3$	**3.16** (4.3)	**3.53** (4.301)	**2.65** (4.31)	**2.62** (4.4)
$m_c^* = 8.0$[d]	$\tau = 500$ y.[h]	$m_{c,0}^* = 4.3$	**3.16** (4.301)	**3.51** (4.32)	**2.75** (4.43)	**1.02** (4.96)

[a] $m_c^* = 7.59$ as in Kagan et al. (2010).
[b] $m_c^* = 7.53$ by Wells and Coppersmith (1994)'s relations.
[c] $m_c^* = 7.5$ like for S. Jacinto fault (Salisbury et al. (2012)).
[d] $m_c^* = 8$ close to that for Northern S. Andreas fault.

[e] $\tau = 250$ like for Northern S. Andreas fault.
[f] $\tau = 100$ like for S. Jacinto fault.
[g] $\tau = 1000$ as in Sieh et al. (1993).
[h] $\tau = 500$ close to a mean value.

List of figure captions

Fig. 1: Time-varying corner seismic moment $M_c(E) = M^*_{c,0} + (M^*_c - M^*_{c,0}) \left[\nu(t-t_0)\right]^2$ as a function of the elapsed time $t - t_0$ between the event (t, M) and the resetting one (t_0, M_0). Panels $a), b)$ and $c)$ are obtained respectively for: fixed $(M^*_c, M^*_{c,0})$ – varying ν, fixed $(\nu, M^*_{c,0})$ – varying M^*_c, fixed (ν, M^*_c) – varying $M^*_{c,0}$. The latter is obtained for a shorter $t - t_0$ interval, because here the differences of the corner seismic moment function can be appreciated: $M_c(E)$ substantially would not change over a longer temporal interval, being M^*_c predominant over $M^*_{c,0}$. Magnitude values are shown in place of seismic moments for an easier interpretation of the figure.

Fig. 2: Surface plots of the time-varying corner seismic moment $M_c(E) = M^*_{c,0} + (M^*_c - M^*_{c,0}) \left[\nu(t-t_0)\right]^2$ as a function of the time elapsed since the reset $t - t_0$ and: the parameter ν with fixed M^*_c in the first line panels, viceversa in the second line. The minimum corner seismic moment is set at $m^*_{c,0} = 4.5$ in each panel.

Fig. 3: Survival function of the TGRE model for several values of the available energy (corner seismic moment), corresponding to the $M_c(E)$ indicated in the legend, in a log-log scale.

Fig. 4: TGRE branching ratio (5) versus its time-varying corner seismic moment, for several values of the difference $\beta_k - \alpha_k$.

Fig. 5: TGR vs TGRE analysis relative to the considered area $\mathcal{A}$, covering the Landers

segment fault, as shown in panel a) (the colored lines with circles represent the nearby segment faults). The temporal interval here is 29 June 1992 - 6 July 1992, that is, within 1 week since the day after the Landers resetting earthquake. The number of events contained in this spatiotemporal window is 437 (red dots in panel a)). Panel b) contains the earthquake cumulative numbers of events inside $\mathcal{A}$ (in red), and outside it (in dark blue). Finally, in panel c) we compare the fit to the data of the TGR model in black, and the TGRE model in yellow, obtained respectively with $m_c^* = 7.59$ and $m_c(E) = 4.301$ (the latter derived from equation (2) with $\alpha = 2$). These corner magnitudes are used also to obtain 1000 simulations of 1000 TGR- and TGRE- distributed seismic moments, respectively, which are plotted as light gray and light yellow cones. The data (red step functions) almost completely fall into the TGRE cone. Magnitude values are shown in place of seismic moments for an easier interpretation.

Fig. 6: The same as Fig. 5, but relative to the temporal interval 29 June 1992 - 29 July 1992, that is, within 1 month since the day after the Landers resetting earthquake. The number of events contained in this spatiotemporal window is 739. The color used for the TGRE model is orange, and $m_c(E) = 4.32$.

Fig. 7: The same as Fig. 5, but relative to the temporal interval 29 June 1992 - 29 September 1992, that is, within 3 months since the day after the Landers resetting earthquake. The number of events contained in this spatiotemporal window is 926. The color used for the TGRE model is green, and $m_c(E) = 4.43$.

Fig. 8: The same as Fig. 5, but relative to the temporal interval 29 June 1992 - 29 June 1993, that is, within 1 year since the day after the Landers earthquake. The number of events contained in this spatiotemporal window is 1120. The color used for the TGRE model is blue, and $m_c(E) = 4.96$.

Fig. 9: Difference between TGRE and TGR log-likelihoods versus the minimum magnitude $m^*_{c,0}$ achieved after the reset.

Figures

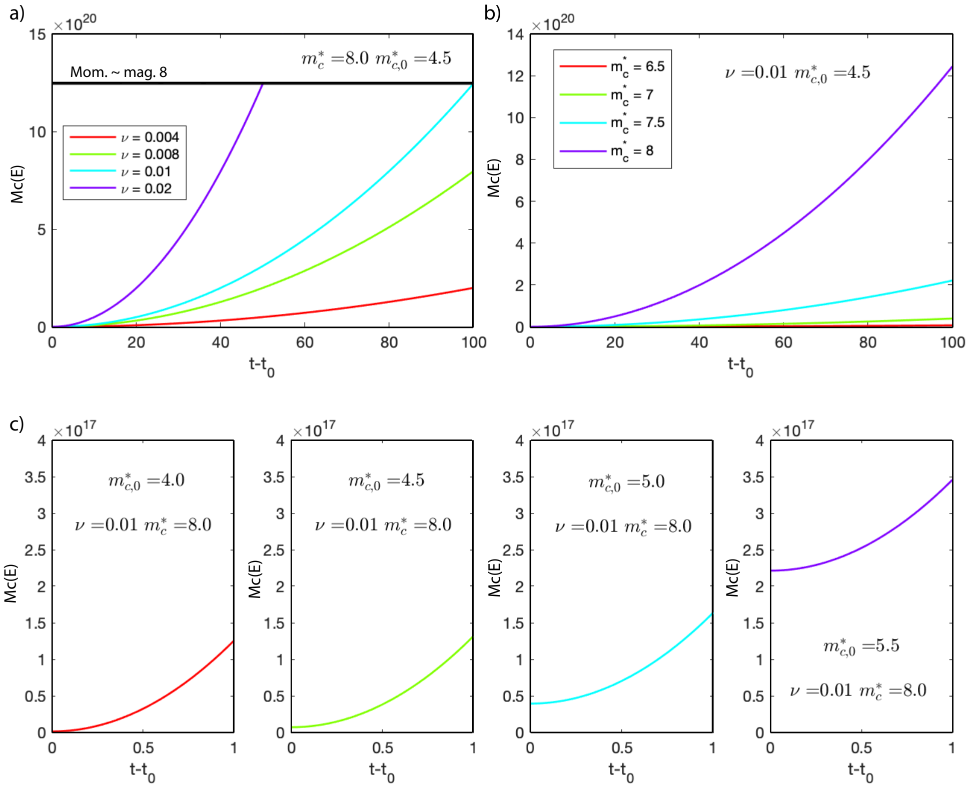

Figure 1: Time-varying corner seismic moment $M_c(E) = M^*_{c,0} + (M^*_c - M^*_{c,0})\,[\nu(t-t_0)]^2$ as a function of the elapsed time $t - t_0$ between the event (t, M) and the resetting one (t_0, M_0). Panels a), b) and c) are obtained respectively for: fixed $(M^*_c, M^*_{c,0})$ – varying ν, fixed $(\nu, M^*_{c,0})$ – varying M^*_c, fixed (ν, M^*_c) – varying $M^*_{c,0}$. The latter is obtained for a shorter $t - t_0$ interval, because here the differences of the corner seismic moment function can be appreciated: $M_c(E)$ substantially would not change over a longer temporal interval, being M^*_c predominant over $M^*_{c,0}$. Magnitude values are shown in place of seismic moments for an easier interpretation of the figure.

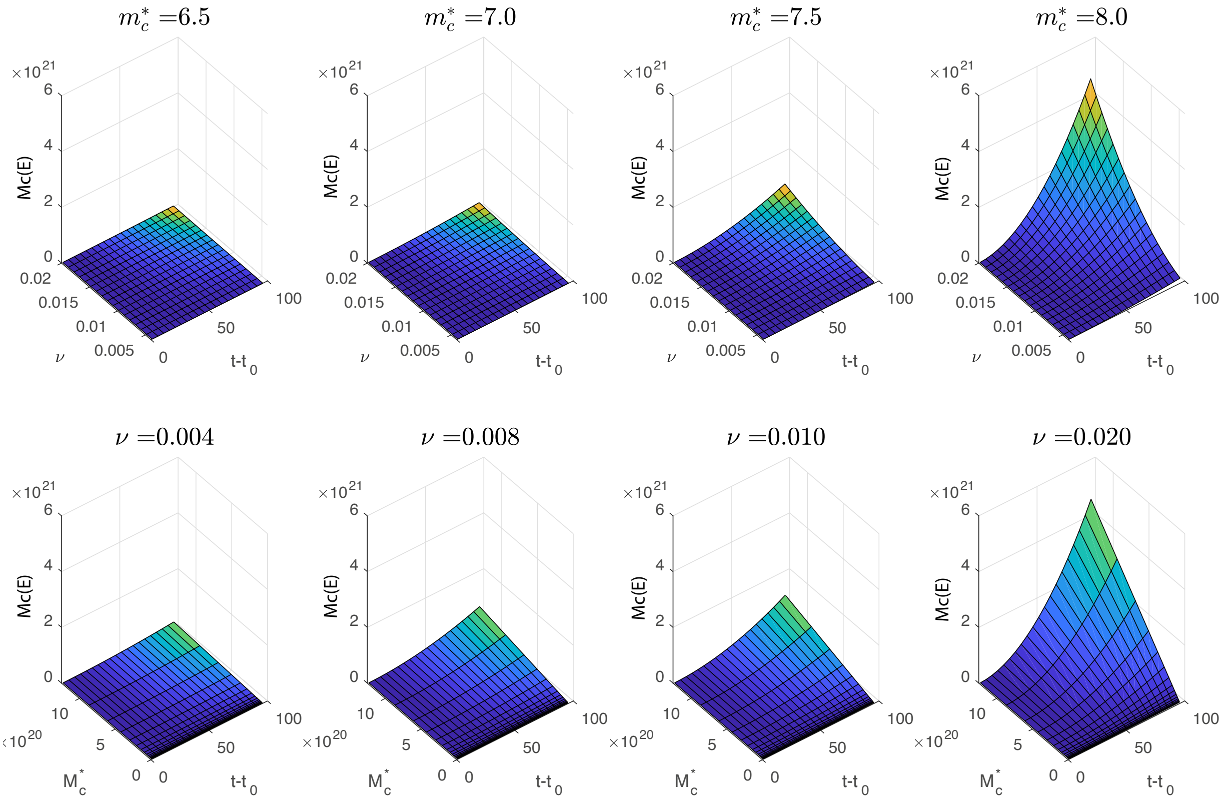

Figure 2: Surface plots of the time-varying corner seismic moment $M_c(E) = M^*_{c,0} + (M^*_c - M^*_{c,0})\,[\nu(t-t_0)]^2$ as a function of the time elapsed since the reset $t-t_0$ and: the parameter ν with fixed M^*_c in the first line panels, viceversa in the second line. The minimum corner seismic moment is set at $m^*_{c,0} = 4.5$ in each panel.

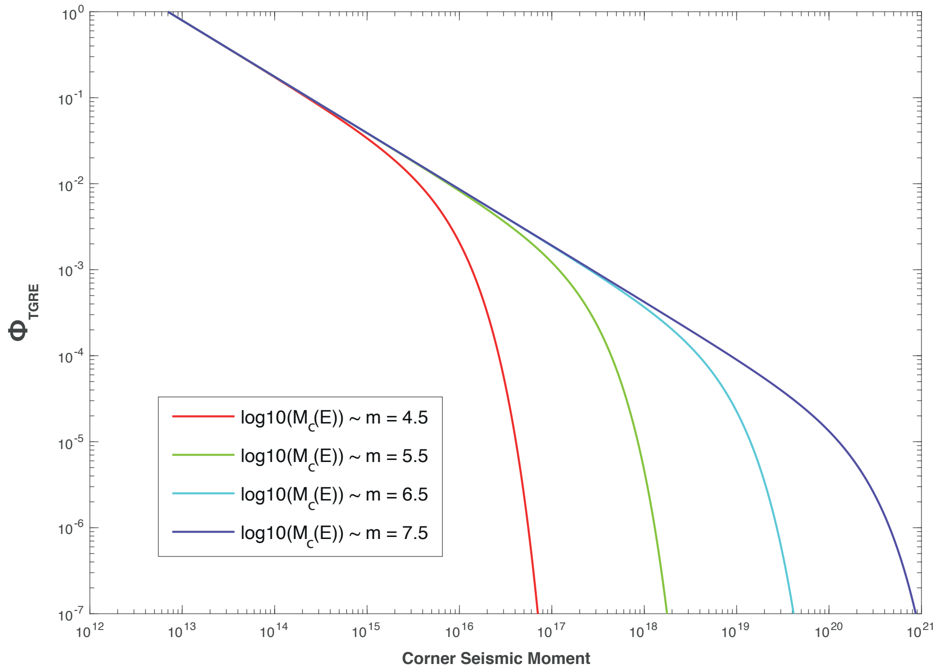

Figure 3: Survival function of the TGRE model for several values of the available energy (corner seismic moment), corresponding to the $M_c(E)$ indicated in the legend, in a log-log scale.

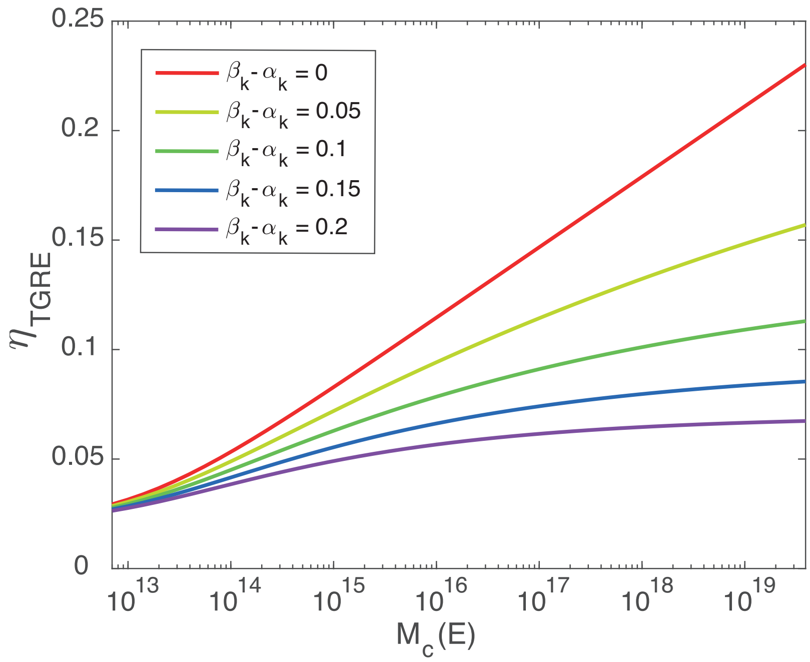

Figure 4: TGRE branching ratio (5) versus its time-varying corner seismic moment, for several values of the difference $\beta_k - \alpha_k$.

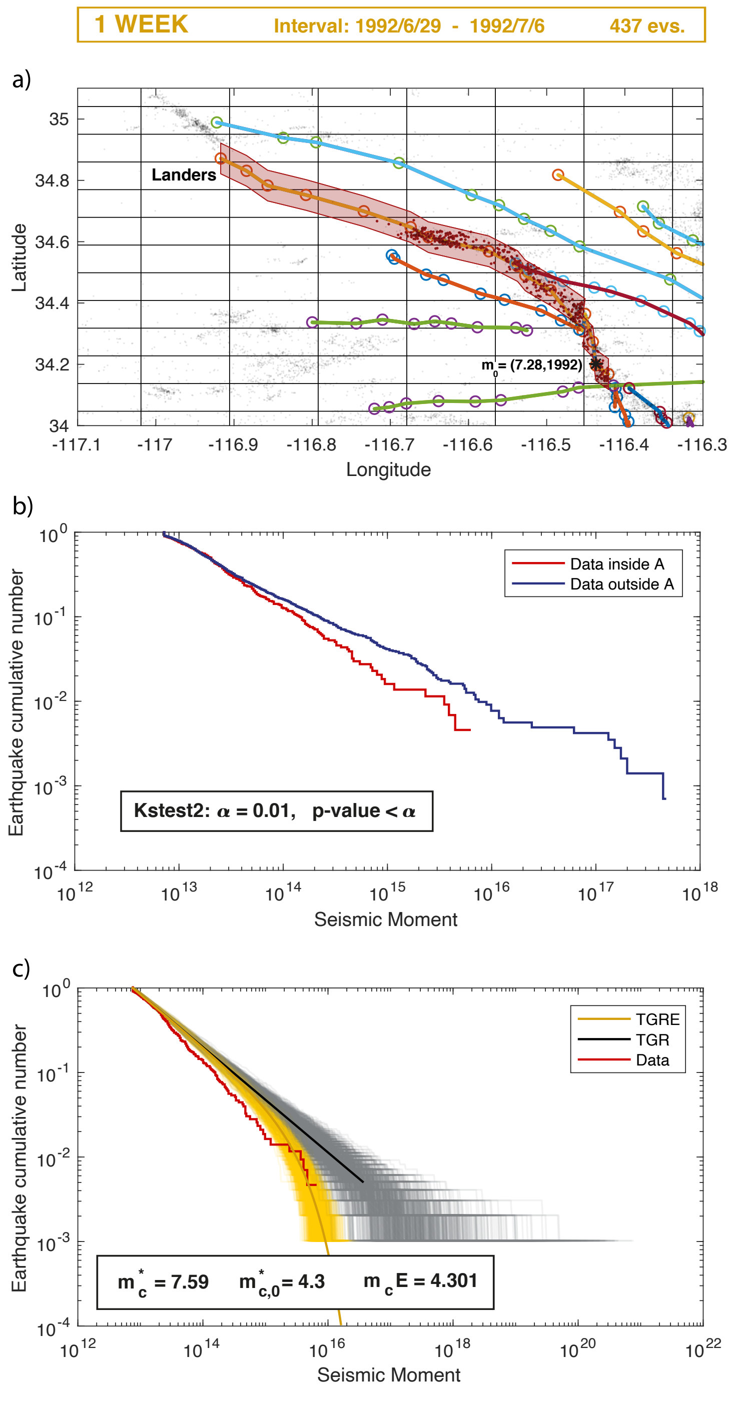

Figure 5: TGR vs TGRE analysis relative to the considered area $\mathcal{A}$, covering the Landers segment fault, as shown in panel *a*) (the colored lines with circles represent the nearby segment faults). The temporal interval here is 29 June 1992 - 6 July 1992, that is, within 1 week since the day after the Landers resetting earthquake. The number of events contained in this spatiotemporal window is 437 (red dots in panel *a*)). Panel *b*) contains the earthquake cumulative numbers of events inside $\mathcal{A}$ (in red), and outside it (in dark blue). Finally, in panel *c*) we compare the fit to the data of the TGR model in black, and the TGRE model in yellow, obtained respectively with $m_c^* = 7.59$ and $m_c(E) = 4.301$ (the latter derived from equation (2) with $\alpha = 2$). These corner magnitudes are used also to obtain 1000 simulations of 1000 TGR- and TGRE- distributed seismic moments, respectively, which are plotted as light gray and light yellow cones. The data (red step functions) almost completely fall into the TGRE cone. Magnitude values are shown in place of seismic moments for an easier interpretation.

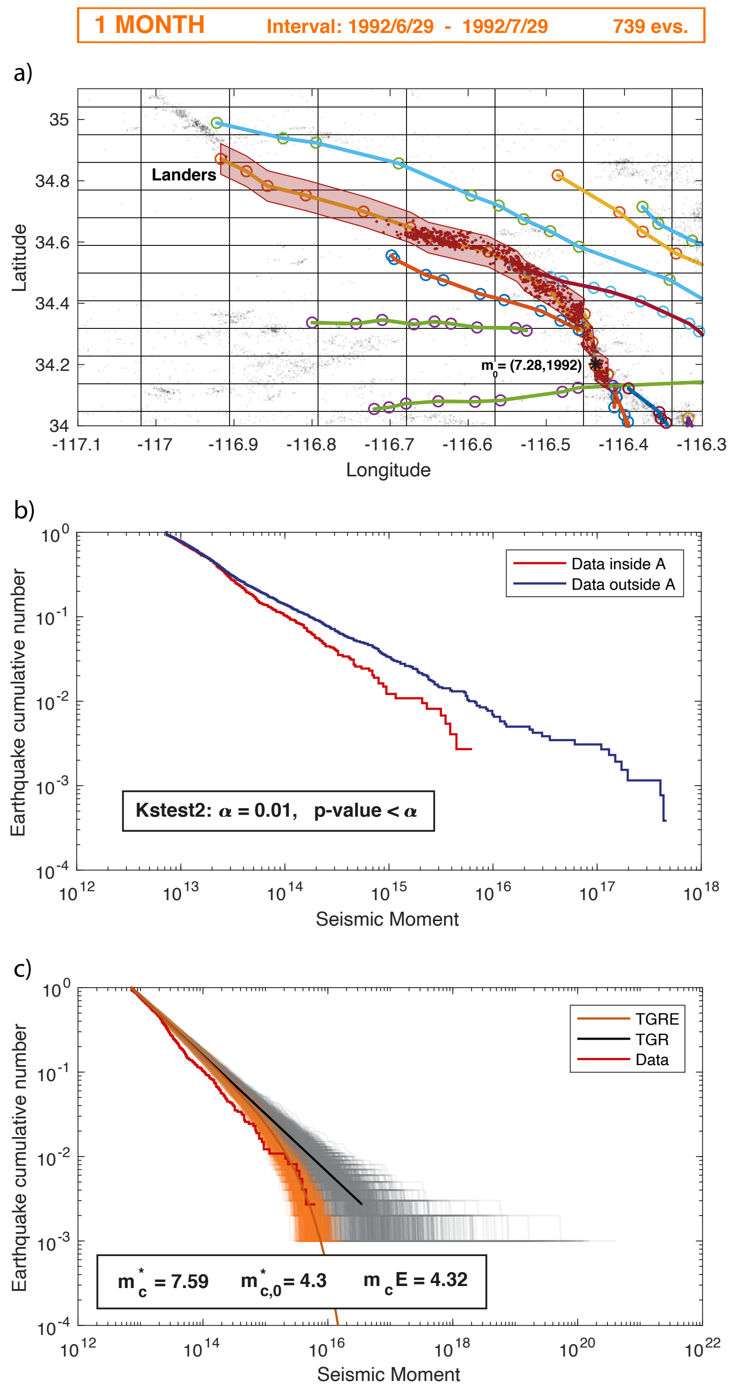

Figure 6: The same as Fig. 5, but relative to the temporal interval 29 June 1992 - 29 July 1992, that is, within 1 month since the day after the Landers resetting earthquake. The number of events contained in this spatiotemporal window is 739. The color used for the TGRE model is orange, and $m_c(E) = 4.32$.

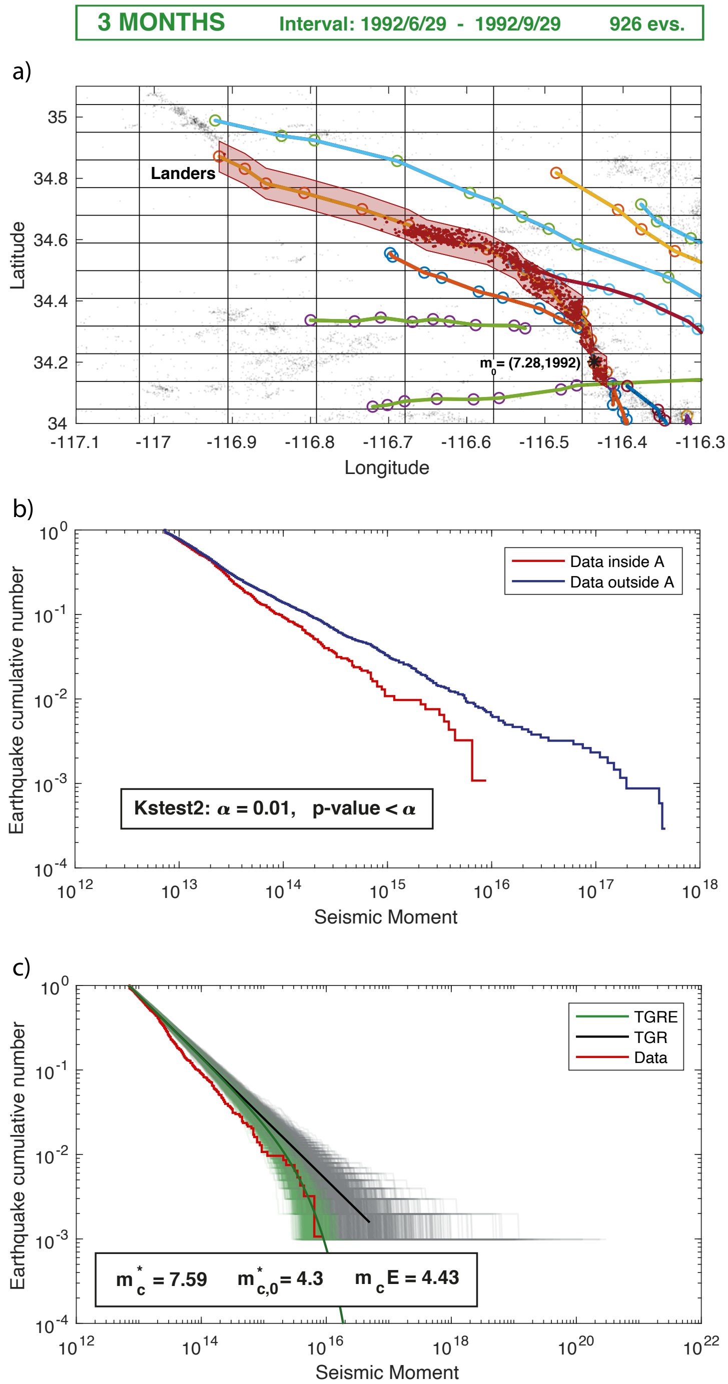

Figure 7: The same as Fig. 5, but relative to the temporal interval 29 June 1992 - 29 September 1992, that is, within 3 months since the day after the Landers resetting earthquake. The number of events contained in this spatiotemporal window is 926. The color used for the TGRE model is green, and $m_c(E) = 4.43$.

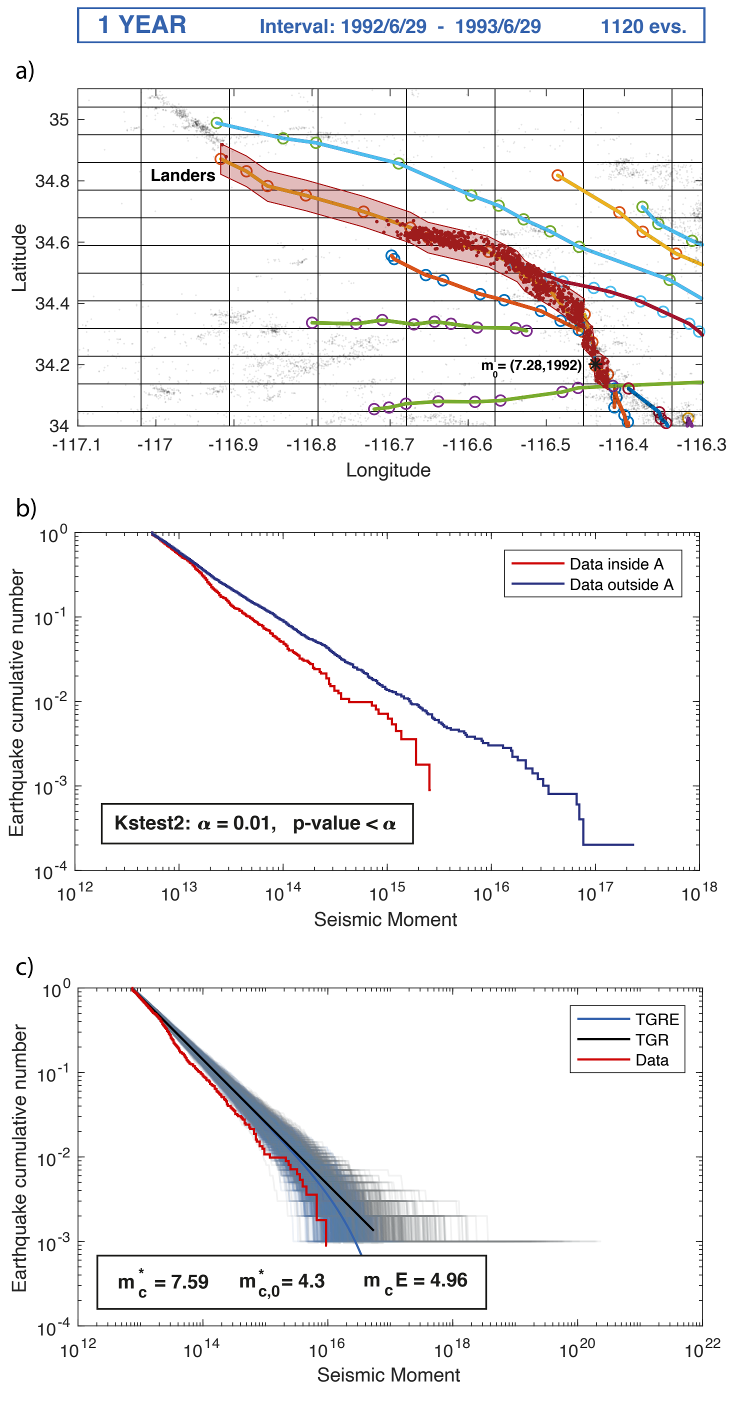

Figure 8: The same as Fig. 5, but relative to the temporal interval 29 June 1992 - 29 June 1993, that is, within 1 year since the day after the Landers earthquake. The number of events contained in this spatiotemporal window is 1120. The color used for the TGRE model is blue, and $m_c(E) = 4.96$.

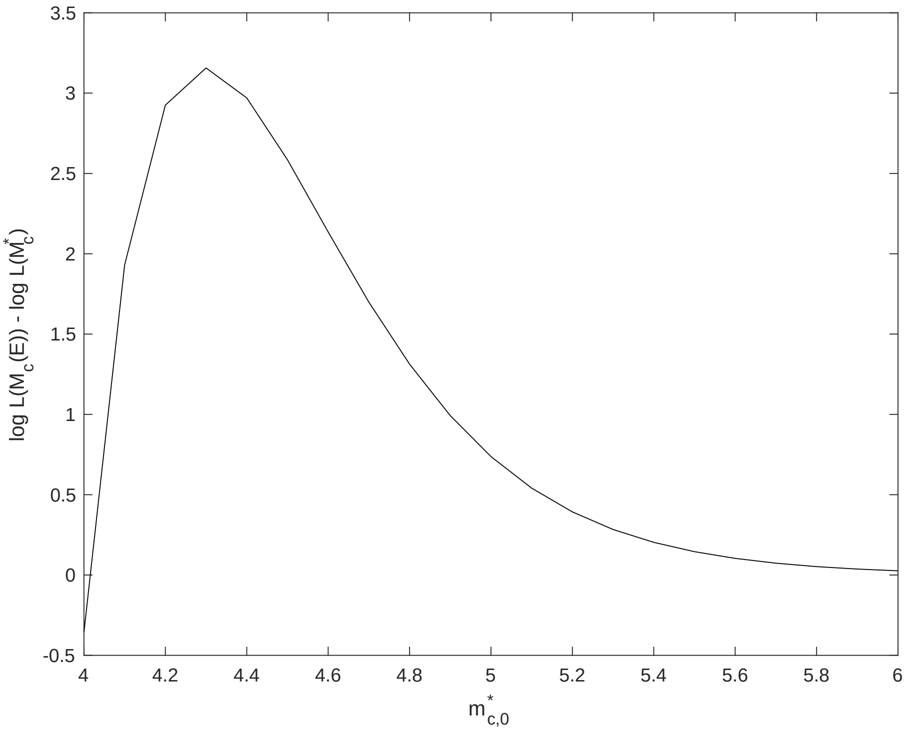

Figure 9: Difference between TGRE and TGR log-likelihoods versus the minimum magnitude $m^*_{c,0}$ achieved after the reset.